Nonlinear Free Energy Relations for Adiabatic Proton Transfer Reactions in a Polar Environment. II. Inclusion of the Hydrogen Bond Vibration

Philip M. Kiefer [†] **and James T. Hynes*** [†,‡]

Department of Chemistry and Biochemistry, University of Colorado, Boulder, Colorado 80309-0215 and Département de Chimie, CNRS UMR 8640 PASTEUR, Ecole Normale Supérieure, 24, rue Lhomond, 75231 Paris, France

Received: September 6, 2001; In Final Form: December 18, 2001

A free energy relationship (FER) between the activation free energy $\Delta G^{\ddagger}$ and the reaction asymmetry ΔG_{RXN} was derived in the preceding paper for acid ionization proton transfer (PT) reactions in a polar environment, in which the proton is treated quantum mechanically, but does not tunnel. In the present paper, the inclusion of the proton donor−acceptor vibration—the vibration of the hydrogen (H−) bond—and its impact on the FER are analyzed. The structure of the resulting FER, which includes quantization of both the proton and the H-bond coordinates, is found to be identical to that for the fixed donor−acceptor case, but with a re-interpretation for certain components, which reflects a significant coupling that exists between the H-bond vibration and the solvent reaction coordinate. This coupling derives from the increased mixing of the reactant and product valence bond electronic structures as the transition state is reached. Analytical expressions for the FER ingredients including these features are obtained. The present description of PT in an H-bond is compared with that of a bond energy-bond order characterization, which is sometimes employed in characterizing condensed phase PT systems. A comparison of the derived FER for PT is also made with the empirical Marcus FER and with other FERs in the literature.

1. Introduction

Rate-equilibrium free energy relations (FER) connecting the reaction activation free energy $\Delta G^{\ddagger}$ with the thermodynamic reaction asymmetry ΔG_{RXN} play a key role in both comprehending and characterizing proton transfer (PT) reactions in solution[1−5] and enzymes.[6,7] In the preceding paper,[8] hereafter labeled I, a FER was derived from an underlying picture of PT reactions which differs considerably from "standard" views.[1,2,9] For example, the acid ionization, or acid−base PT reaction within a hydrogen (H−) bonded complex

$$AH\cdots B \rightleftharpoons A^{-}\cdots HB^{+} \tag{1.1}$$

is described as driven by configurational changes in the surrounding polar environment; the reaction activation free energy is largely determined by the reorganization of this environment (such that the reaction coordinate is a solvent coordinate), together with certain zero point energy (ZPE) changes associated with the quantized proton motion. By contrast, traditional approaches would instead focus on the height of any potential barrier in the coordinate of the transferring proton. In the adiabatic PT picture described in I, the fast vibration of the proton adiabatically follows the slower rearrangement of the environment, and one considers the instantaneous proton potential for different arrangements of the environment. The underlying electronic description of the system is a two Valence Bond (VB) state basis

$$|\Psi\rangle = c_N|\Psi_N\rangle + c_I|\Psi_I\rangle \tag{1.2}$$

involving neutral (N) and ionic (I) structures, along the lines of the Mulliken picture of PT reactions.[10−12] Strong electronic coupling between these VB states produces the ground electronically adiabatic surface on which the reaction occurs.

The principal result of I—derived for the regime of quantum adiabatic (nonclassical but nontunneling) PT described at length there and for a fixed proton donor−acceptor separation, i.e., fixed H-bond coordinate—is the nonlinear FER connecting the reaction barrier with the reaction asymmetry (eq 5.46 of I)

$$\Delta G^{\ddagger} = \Delta G_o^{\ddagger} + \alpha_o \Delta G_{RXN} + \alpha_o' \frac{(\Delta G_{RXN})^2}{2} \tag{1.3}$$

with molecular expressions given for its ingredients. $\Delta G_o^{\ddagger}$ is the "intrinsic" reaction barrier, $\Delta G_o^{\ddagger} = \Delta G^{\ddagger}(\Delta G_{RXN} = 0)$, i.e., the activation free energy for the reference thermodynamically symmetric reaction; α_o is the derivative of the reaction barrier with respect to ΔG_{RXN}, i.e., the Brønsted coefficent, evaluated at $\Delta G_{RXN} = 0$; and finally, α_o' is the Brønsted coefficent slope evaluated at $\Delta G_{RXN} = 0$. The intrinsic free energy barrier is composed of a contribution due to a certain solvent reorganization $\Delta G_{m,o}^{\ddagger}$ and the difference in the ZPE $Z_o^{\ddagger} - Z_o^R$ of the proton between the reactant and transition state for the symmetric reaction (eq 5.38 of I)

$$\Delta G_o^{\ddagger} = \Delta G_{m,o}^{\ddagger} + Z_o^{\ddagger} - Z_o^R \tag{1.4}$$

The Brønsted coefficient for the symmetric reaction was found to be $\alpha_o = 0.5$, a result arising from the feature that the electronic structure of the transition state in the solvent coordinate for the symmetric reaction contains equal contribu-

* To whom correspondence should be sent. Phone: (303) 492−6926. Fax: (303) 492−5894. E-mail: hynes@spot.colorado.edu.
[†] Department of Chemistry and Biochemistry, University of Colorado.
[‡] Département de Chimie, CNRS UMR 8640 PASTEUR, Ecole Normale Supérieure.

10.1021/jp013425w CCC: $22.00
Published on Web 02/08/2002

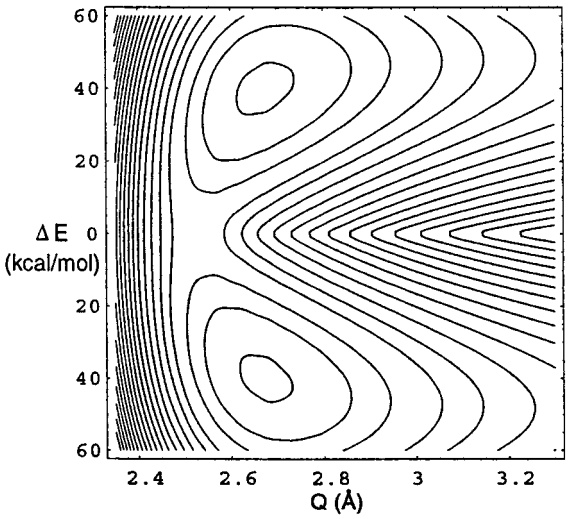

Figure 1. Contour plot of the PT system free energy versus the solvent coordinate, ΔE, and the H-bond coordinate separation, Q, for a symmetric reaction. Contour spacings are set at 1 kcal/mol.

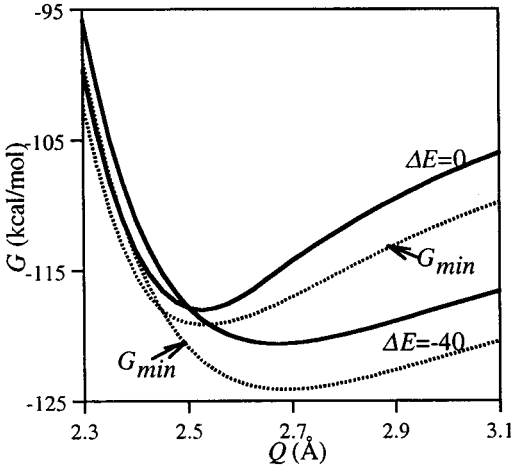

Figure 2. Cuts of the two-dimensional surface in Figure 1, at two different solvent coordinate values $\Delta E = 0$ (‡) and $\Delta E = -40$ kcal/mol (R) (solid lines). Also shown for later reference are G_{min} cuts (dotted lines) for the same solvent values $\Delta E = 0$ and $\Delta E = -40$ kcal/mol. G_{min} is the free energy of the system at the minimum of the proton potential, the classical equilibrium position of the proton. The difference between G and G_{min} is the ZPE of the proton (cf. eq 2.14 of I).

tions from both electronic resonance structures representative of the reactant and product states. The slope of the Brønsted coefficient is (eq 5.44 of I)

$$\alpha' = \alpha'_o = \frac{1}{(\Delta E^P - \Delta E^R)^2}\left(\frac{1}{k^{\ddagger}} + \frac{1}{k_R}\right) \qquad (1.5)$$

where k_R and $k^{\ddagger}$ are the force constants for the free energy variation in the solvent reaction coordinate ΔE, defined in I, at the reactant and transition state, and $\Delta E^P - \Delta E^R$ is the separation of the product and reactant states in that coordinate.

In the present paper, we extend this perspective and analytical theory to include the H-bond vibration, i.e., that involving the separation of the proton donor and acceptor A and B in eq 1.1. As will be seen, a structure for $\Delta G^{\ddagger}$ identical to that given above results, with a re-interpretation of certain components to apply to the variable H-bond coordinate case.

The importance of this H-bond vibration for an adiabatic PT reaction is best shown by focusing on its influence on the proton barrier at the transition state (TS) configuration of the environment (illustrated in Figure 2 of I): the barrier in the proton coordinate will increase as the donor−acceptor separation—hereafter Q—is increased because a higher energetic price must be paid on the way to breaking the original bond before the energetic gain from the new bond formation is realized. The PT reaction must thus be considered not only in the presence of a proton potential whose asymmetry is fluctuating due to the environment—as extensively described in I—but whose height is also fluctuating due to the H-bond coordinate motion. There is little previous detailed analysis of the H-bond coordinate's influence in the proton adiabatic regime considered here. Aspects of this have been analyzed by Staib et al.,[13,14] and signatures of its influence are visible in the surfaces presented in ref 15, though not analyzed. In any event, its influence on FERs has not been considered previously. The present paper relies considerably on I, and we repeat a few of the most important equations from I for the reader's convenience. As in I, we note that the particular proton adiabatic description we employ (ground vibrational state of the proton) is appropriate for relatively low barrier reactions. Further, we again restrict our consideration to what we termed "intrinsically symmetric reactions" (cf. section 3 of I), where any reaction asymmetry arises solely from a finite reaction free energy. We will return to both of these issues at the paper's conclusion.

The outline of the remainder of this paper is the following. Section 2 deals with the free energy surface's overall characteristics and the quantization of the Q vibration. A comparison of the present perspective's results with that of a bond energy-bond order description[16,17] is also given there. The activation free energy-reaction free energy relationship is analyzed in section 3, including a comparison of the derived FER with the empirical Marcus FER,[2] as well as with other FERs.[4,7,13,18−20] Concluding remarks are offered in section 4.

2. General Perspectives for PT Reaction with H-bond Vibration Included

2a. Features of the PT Free Energy Surface. Although we will ultimately quantize the H-bond Q motion, it proves useful to first discuss the PT free energy surface as an explicit function of Q, to appreciate the essential aspects of its Q dependence and in particular, aspects related to the coupling of Q and the solvent coordinate. Figure 1 is a contour plot of the *proton-quantized* (ground vibrational state) free energy surface $G(Q, \Delta E)$ for a thermodynamically symmetric reaction, generated with the formalism and parameters presented in I for PT, eq 1.1, between an oxygen donor and acceptor. (For clarity and discussion, Figure 3 in I is reproduced here as Figure 1). ΔE is the collective solvent coordinate extensively described in I (cf. eq 2.9). The surface exhibits both a reactant (R) and a product (P) well, stable minima each with equilibrium donor−acceptor separations $Q \approx 2.7$ Å. The floors of the valleys in the solvent coordinate are more narrowly separated as Q decreases leading to the surface's saddle point. This saddle point, located at $\Delta E = 0$ and $Q \approx 2.5$ Å, a value of Q compressed compared to that for R and P, would define a TS surface in the perspective that Q is classical. Figure 1 also shows the important feature that the H-bond vibration frequency varies with the reaction coordinate ΔE, increasing as the saddle point region is approached from either the R or P side.

These aspects indicating a strong coupling between the H-bond coordinate features of the surface and the solvent coordinate are further highlighted via Figure 2 (solid lines), which shows two cross-sections of the Figure 1 surface, i.e.,

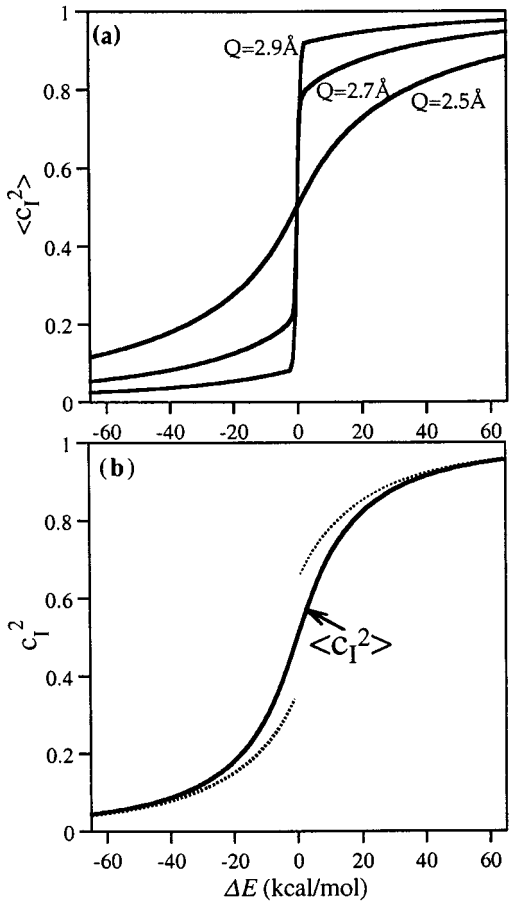

Figure 3. (a) Proton ground state vibrationally averaged ionic electronic structure composition $\langle c_I^2 \rangle$ vs the solvent coordinate ΔE at three different values of the donor−acceptor separation Q, 2.5, 2.7, and 2.9 Å. (b) Ground-state vibrational (proton and H-bond vibrational mode) average $\langle c_I^2 \rangle$ vs. ΔE (solid line), and $c_I^2(q_{min}, Q_{min}, \Delta E)$ (dotted line) vs ΔE .

the H-bond vibrational potential for the TS and reactant, $\Delta E = 0$ and -40 kcal/mol, respectively. For the former, the curve has an equilibrium separation $Q \approx 2.5$ Å and a frequency 550 cm^{-1}, whereas the latter curve has a larger equilibrium separation, $Q \approx 2.7$ Å, with a much lower frequency, 290 cm^{-1}. Although these features are of course consistent with the general expectation that H-bonds are stronger at smaller bond lengths,[21] a deeper analysis is useful.

We first focus on the variation with Q of the equilibrium positions of the R and P solvent configurations apparent in Figure 1, which we label as ΔE^R and ΔE^P. At very large Q, the separation of the minima is relatively constant. As Q is decreased, the relative distance between ΔE^R (ΔE^P) and $\Delta E = 0$ decreases. This behavior arises from the changing electronic character of the reactants and products, and has its ultimate source in a significant electronic coupling, which mixes the R and P diabatic states to give the electronically adiabatic state. The critical positions ΔE_c for $G(Q, \Delta E)$ are given by (cf. eq 5.29 of I)

$$\Delta E_c = -K(\mu_N - \mu_I)^2\left(\frac{1}{2} - \langle c_I^2(\Delta E_c)\rangle\right) - \Delta G_d \quad (2.1)$$

where K is a solvent force constant and ΔG_d is the free energy difference between the reactant and product electronic diabatic states, whose dipole moments are μ_N and μ_I, respectively. Here, the ionic character, i.e., (cf. eq 2.11 of I)

$$c_I^2 = \frac{1}{2} + \frac{1}{2}\frac{(\Delta E + U_N - U_I)}{\sqrt{(\Delta E + U_N - U_I)^2 + 4\beta^2}};\ c_N^2 + c_I^2 = 1 \quad (2.2)$$

is averaged over the ground state of the proton vibration $\langle c_I^2 \rangle$. The Q dependence in eq 2.2 is contained in the electronic coupling β—described in section 3 of I, and which exponentially increases as Q decreases ($-\beta = -35 \exp(-1.5(Q - 2.55\ \text{Å}))$ kcal/mol)—as well as in the difference between the energies of the vacuum R and P diabatic states $U_N - U_I$, which decreases with decreasing Q. Both trends tend to make the R and P states less and less like the pure VB states as Q is decreased, due to a stronger coupling between states with a smaller gap, and the separation of their locations in ΔE diminishes, as we now describe in more detail.

The detailed discussion of the above qualitative point can be effected in terms of $\langle c_I^2 \rangle$ because eq 2.1 shows that the variation in the R and P minima in the solvent coordinate arises from its Q dependence. Figure 3a displays $\langle c_I^2 \rangle$ versus ΔE for various fixed Q values. It is useful for reference to note that at $\Delta E = 0$, the proton—quantum averaged over its motion—is always equally shared between donor and acceptor, and $\langle c_I^2 \rangle = 0.5$ is independent of Q, a feature characteristic of the saddle point region. To understand the variation of $\Delta E^P - \Delta E^R$ with Q, we need to focus on the behavior of $\langle c_I^2 \rangle$ in the R and P "wings" of Figure 3a as a function of Q. For large Q values the electronic coupling β is negligible compared to the gap $|\Delta E_c + U_N - U_I|$ in eq 2.2, so that the R and P states are nearly the pure VB states at each Q value in this range: $\langle c_I^2 \rangle \approx 0$ for the reactant and $\langle c_I^2 \rangle \approx 1$ for the product, and both the R and P locations $\Delta E^{R,P}$ and the distance between them $\Delta E^P - \Delta E^R$ are independent of Q. As Q decreases, β increases and the gap $|\Delta E_c + U_N - U_I|$ decreases, so that the mixing of the VB electronic states for R and P states increases; thus the electronically adiabatic R state has somewhat more ionic character, $\langle c_I^2 \rangle > 0$, and the P state has somewhat less, $\langle c_I^2 \rangle < 1$. Consequently, the R and P states become more electronically similar, and the distance between them in the solvent coordinate ΔE decreases, thus accounting for the first feature, we noted in Figure 1.[22]

We next focus on the difference in H-bond frequency between R (P) and TS. As shown in Figure 2, the increase in this frequency going from R to TS for the full free energy G is mimicked by that for G_{min}, the free energy when the proton is at its classical position for a given Q and ΔE. G minus G_{min} is thus the quantum zero point energy for the proton. The frequency difference can then be understood by focusing on that for G_{min} at R and TS. To this end, we rewrite G_{min} ignoring Q independent terms (cf. eq 5.3 in I)

$$G_{min}(Q,\Delta E) \approx V_Q(Q) + \frac{V_N + V_I}{2} - \frac{1}{2}\sqrt{(V_N - V_I + \Delta E)^2 + 4\beta^2} \quad (2.3)$$

where V_N and V_I are evaluated at $q = q_{min}$. The first term V_Q, which is independent of ΔE, is a primarily repulsive donor -acceptor potential, and dominates the repulsive branch of G_{min} in Figure 2, whereas the last two terms containing the electronic diabatic proton potentials for the ionic state V_I and neutral state V_N (cf. eq 3.1 of I) describe the attractive branch of G_{min}. As ΔE goes toward zero, the electronic coupling's Q dependence contributes more (negatively) to the attractive branch; accordingly, the frequency of G_{min} increases as the attractive branch steepens going from R to TS.[23]

In summary, the H-bond−solvent coordinate coupling arises from the increased mixing of the electronic character between the reactant ionic and the product neutral states as Q decreases. This mixing's impact is most important near the TS, where it is quite sensitive to the H-bond separation. The result is a higher H-bond vibrational frequency near the TS compared with the reactant and product states. The $Q-\Delta E$ coupling and increase in Q vibrational frequency near the TS combine to explain another behavior exhibited in Figure 1, namely, the increase in the solvent barrier as Q increases: the difference in electronic structure $\langle c_I^2 \rangle$ between the reactant and transition states increases and the free energetic cost for solvent rearrangement is correspondingly larger. We will return to this issue in section 3c.

2b. Quantization of the H-Bond Vibration. The H-bond frequencies are sufficiently high, particularly near $\Delta E = 0$, such that the H-bond Q vibration should be quantized. Here, we follow Staib et al. [13] and quantize Q for each fixed solvent configuration ΔE in an adiabatic Born−Oppenheimer (BO) description. In principle, this assumes an H-bond vibration time scale short compared to the important characteristic time scales associated with the solvent coordinate, a condition really only fairly necessary near the reaction TS, where solvent dynamical effects which would cause transitions between the different Q vibrational states in the passage through the transition state are excluded;[13] away from the TS, such transitions will in fact be common, and indeed are required[13] in order to have an equilibrium distribution of the Q vibrational states so that one can discuss a well-defined overall PT rate constant in terms of a thermally weighted contribution of the PT rate constants in each of the Q vibrational states, as defined below.[24]

The Hamiltonian defining the H-bond vibrational motion is

$$\hat{H}_Q = \hat{K}_Q + G(Q,\Delta E) \tag{2.4}$$

where $\hat{K}_Q$ is the Q mode's kinetic energy operator. The Q coordinate Schrödinger equation is solved in the BO approximation to generate the system free energy levels $G_i(\Delta E)$ and H-bond vibrational wave functions $\Phi_i(Q; \Delta E)$

$$\hat{H}_Q|\Phi_i(Q;\Delta E)\rangle = G_i(\Delta E)|\Phi_i(Q;\Delta E)\rangle \tag{2.5}$$

$G_i(\Delta E)$ represents the system free energy, at fixed solvent coordinate ΔE, with the quantized proton in its ground vibrational state and the H-bond $A-B$ vibration in its ith vibrational state.

Figure 4 displays the resulting calculated $G_i(\Delta E)$, as a function of the solvent coordinate, for the ground, first, and second excited states for the H-bond vibration. The reaction barrier height is larger for excitations of the latter. In a simplified harmonic description, this is due to the higher H-bond frequency at the TS $\Delta E = 0$ compared to that in the R well, so that the effective barrier height approximately doubles for $i = 1$ compared to $i = 0$; the anharmonicity apparent in the Q potentials in Figure 2 reduces this somewhat.

Thermal activation of the H-bond vibration would then result in a higher effective barrier than for the ground-state curve, and except for the special case where the H-bond vibrational frequency is small compared with the thermal energy RT, the effective reaction barrier will typically be well represented by the solvent barrier on the ground H-bond vibrational curve, a feature to be confirmed presently.

Within the assumption that thermal equilibrium is maintained over the distribution of reactant region H-bond vibrational states,

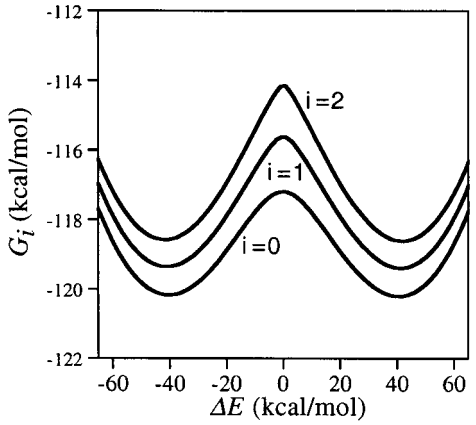

Figure 4. Free energy curves with the quantized proton in its ground vibrational state and the quantized H-bond vibrational mode in the ground, first excited, and second excited energy states, versus the solvent coordinate ΔE for a symmetric PT reaction.

the overall rate constant is just an appropriate thermal average of the individual rate constants

$$k_i = \frac{\omega_s^i}{2\pi}\exp(-\Delta G_i^{\ddagger}/RT) \tag{2.6}$$

Here $\omega^i{}_s$ is the solvent frequency—the frequency of ΔE motion in the ith reactant well—and the ith state free energy barrier height is $\Delta G_i^{\ddagger} = G_i(\Delta E_i^{\ddagger}) - G_i(\Delta E_i^R)$ for which the free energy for each reactant H-bond vibrational state is defined at the minimum in the reactant region $\Delta E^R{}_i$. The solvent reactant well frequency does not differ significantly in different populated states, so that the thermal rate constant can be written as

$$k_{\mathrm{PT}} = \sum_{i=0}^{\infty} P_i K_i = \frac{\omega_s}{2\pi}\sum_{i=0}^{\infty} P_i \exp(-\Delta G_i^{\ddagger}/RT) \tag{2.7}$$

in which the thermal probability for being in each reactant H-bond vibrational state is $P_i = \exp(-G_i/(\Delta E_i^R)/RT)/\sum_i \exp(-G_i(\Delta E_i^R)/RT)$.

We anticipated above that the average rate constant will be dominated by the ground H-bond-vibrational state rate constant, and that the effective barrier height and reaction thermicity will be similar to that in this ground state. We examine this issue by plotting the free energy relation in a manner similar to that for fixed Q (see Figure 6 of I). In particular, the effective activation free energy—which includes the thermally weighted contributions of the ground and excited H-bond vibrational states—is obtained via the natural logarithm of the sum in eq 2.7

$$\Delta G_{\mathrm{eff}}^{\ddagger} = -RT\ln(\sum_i P_i \exp(-\Delta G^{\ddagger,i}/RT)) \tag{2.8}$$

The expression for the effective reaction asymmetry is similar; it is proportional to the natural logarithm of the ratio of the partition functions for the product and reactant

$$\Delta G_{\mathrm{RXN}} = -RT\ln(\sum_i \exp(-\Delta G_i^P/RT)/\sum_i \exp(-\Delta G_i{}^R/RT)) \tag{2.9}$$

Figure 5 displays the calculated $\Delta G^{\ddagger}{}_{\mathrm{eff}}$ vs. ΔG_{RXN} profile at $T = 300$ K, as well as the comparison value of $\Delta G^{\ddagger}$ vs. ΔG_{RXN} for PT exclusively in the ground H-bond vibrational state i=0. Both display nonlinear FER relationships qualitatitively similar

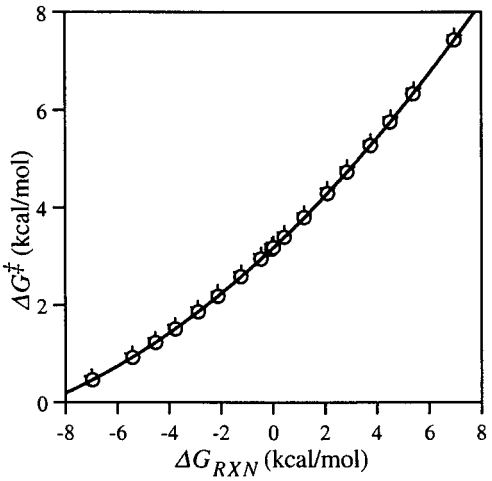

Figure 5. PT activation- reaction free energy relationship $\Delta G^{\ddagger}_{\text{eff}}$ vs. ΔG_{RXN}, including thermally excited H-bond vibrational states(+). The free energy behavior for the ground H-bond vibrational state is also shown(o). The line is eq 1.3, with $\Delta G^{\ddagger}_{o} = 3.17$ kcal/mol, $\alpha_o = 0.5$, and $\alpha'_o = 0.032$ mol/kcal.

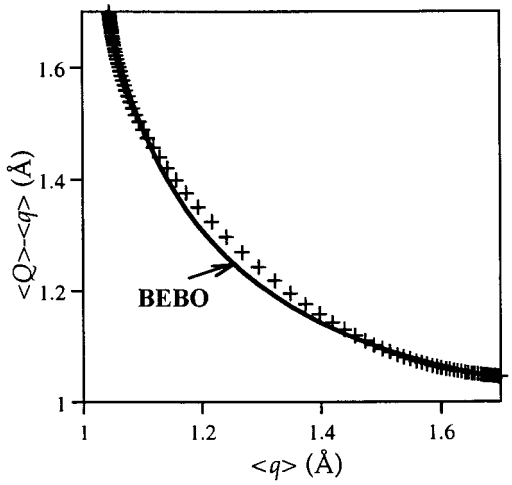

Figure 6. Comparison with a BEBO perspective. Calculated quantum averages $\langle Q - q\rangle$ vs $\langle q\rangle$ for the O···O systems discussed in section 2. Each point represents a specific value of ΔE. The line is the fit to eq 2.11: $r_o = 0.97$ Å and $b = 0.40$ Å.

to the behavior displayed in Figure 6 of I. The close agreement between the ground H-bond vibrational state result and that including all H-bond vibrational states shows that the PT rate is dominated by reaction in the ground state, and we will restrict all of our further analysis to this state. Finally, the line in Figure 5 shows that for the ground vibrational state, the FER eq 1.3, provides an excellent description. We will discuss this success further in section 3.

2c. Comparison with Bond Energy-Bond Order Perspective. It is important to note that the coupling between the proton potential asymmetry, determined by the solvent coordinate ΔE, and the H-bond distance discussed in section 2a is consistent with experimental neutron diffraction[16] and NMR[17] measurements for the geometries of hydrogen bond systems with different *equilibrium* symmetries, as opposed to our focus on geometric evolution *during* a PT reaction. In connection with these experiments, this correlation has been characterized in a different way, via the bond-energy bond order (BEBO) perspective,[25] in which the sum of the order of the proton-donor and proton-acceptor bonds is set equal to unity, resulting in the relation

$$\exp[-(Q - q - r_o)/b] + \exp[-(q - r_o)/b] = 1 \qquad (2.10)$$

with $r_o = 0.93$ Å and $b = 0.39$ Å for OH··O systems and $r_o = 0.99$ Å and $b = 0.40$ Å for NH···N systems.[16,17] Ordinarily, this relation is written[16,17,25] in terms of the proton and H-bond coordinates themselves, i.e., in a completely classical perspective, and within the "standard" perspective, it would describe the contributions of Q and q to the classical reaction path. The barrier for this classical path is the energetic cost of breaking and forming a bond with the proton. At the classical transition state in the q and Q coordinates for a symmetric reaction, the bond order is 0.5 for each bond, so that the proton is equally attracted to the donor and acceptor, compressing the donor−acceptor distance. One might think that there would be no remnant of such a pathway in the present fully quantum approach, but we now show that this is not the case.

To examine the situation in the present perspective, where those vibrations are quantized, we instead will consider a generalization of eq 2.10, in which the quantum nuclear averages for Q and q are inserted in eq 2.10

$$\exp[-(\langle Q - q\rangle - r_o)/b] + \exp[-(\langle q\rangle - r_o)/b] = 1 \qquad (2.11)$$

Figure 6 displays the curve, calculated for the present system, of the quantum averages $\langle Q - q\rangle$ vs $\langle q\rangle$, where the quantum averages are taken over the ground states of both the H-bond Q and proton q vibrations; each point, i.e., each pair of $\langle Q - q\rangle$ and $\langle q\rangle$ values, represents those values evaluated for a specific value of the solvent coordinate ΔE. A PT reaction proceeds with $\langle Q - q\rangle > \langle q\rangle$ (top left of Figure 6) to the TS with $\langle Q - q\rangle \approx \langle q\rangle$, and then on to products where $\langle Q - q\rangle < \langle q\rangle$. The points in Figure 6 are then fit to the BEBO-based eq 2.11. The result (solid line) is similar to that obtained experimentally, with $r_o = 0.97$ Å and $b = 0.40$ Å, and indeed the general correspondence between points and eq 2.11 is rather striking.

From the present perspective, the constructed BEBO plot describes the quantum average of the nuclear vibrations throughout the course of the reaction. The compression in $\langle Q\rangle$ is a result of the electronic structure shift between the neutral and ionic states at the TS. A distinct difference between eq 2.11 and the data occurs in the TS region, where the points portray a more flat trend compared to the curved BEBO behavior. The difference arises from the delocalized quantum character of the proton wave function. To illustrate this point, Figure 7 displays the proton ground vibrational wave function for the TS for three possibilities. It is convenient to discuss first the most familiar quantum limit, tunneling (Figure 7a). In nonadiabatic tunneling, the proton potential at the transition state in the solvent coordinate is a symmetric double well potential, with the proton ground vibrational state below the proton barrier. The proton thus must tunnel to get from the reactant proton well to the product proton well. The shift in localization of the proton from the R to the P via tunneling, with a double lobe character of the wave function at the TS, would lead to an abrupt corner-cutting behavior[26,27] in a $\langle Q - q\rangle$ vs $\langle q\rangle$ plot. As the reaction becomes adiabatic, with the ground vibrational state of the proton now above the barrier of the double well potential at the TS, the proton wave function still contains a dual lobe character caused by a double well potential (Figure 7b). Consequently, the corner-cutting aspect is still present but is softened. This contrasts with the extreme adiabatic case where the proton potential at the TS is a single well (Figure 7c). The proton wave function is single lobed, and $\langle q\rangle$ would thus shift more slowly at the TS, resulting in a more curved plot.

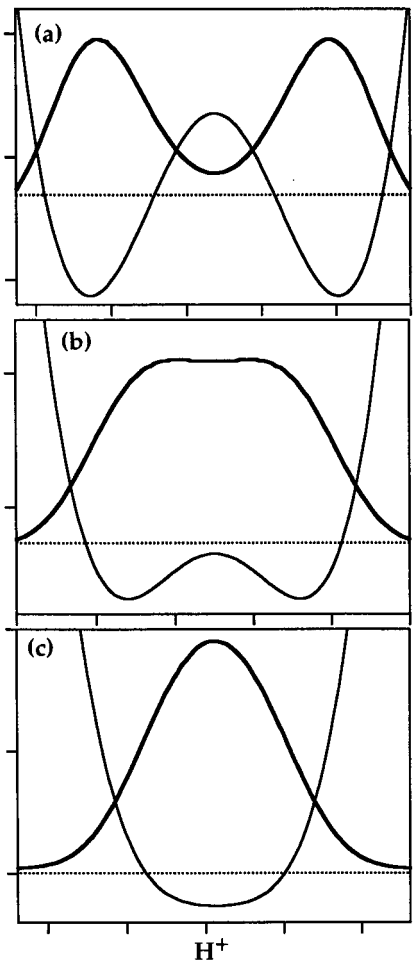

Figure 7. Proton wave functions for TS proton potential for (a) nonadiabatic PT (i.e., tunneling), (b) adiabatic PT, with dual lobe character, and (c) deep adiabatic PT, with single lobe character. Dotted lines indicate the proton ground vibrational energy level.

3. Activation-Reaction Free Energy Relation Analysis

The dominance of the ground H-bond vibrational state contribution in the rate expression eq 2.7 allows us to focus on only this level, and to derive a $\Delta G^{\ddagger} - \Delta G_{RXN}$ relation in a manner completely analogous to that given for the fixed Q case in I. Our orienting discussion in section 2 was presented via two successive BO approximations, quantizing first the proton coordinate q—which provided the free energy $G(Q,\Delta E)$ discussed at length in I—and then quantizing Q. To proceed in a fashion which is most efficient and convenient in exploiting the previous results of I, we will now instead quantize these two coordinates *simultaneously* in a BO approximation with respect to the slow solvent coordinate by solving the two-dimensional Schrödinger equation, parametric on ΔE

$$\hat{H}_{q,Q}|\varphi_{q,Q}\rangle = [\hat{K}(q,Q) + \hat{G}(q,Q;\Delta E)]|\varphi_{q,Q}\rangle = G(\Delta E)|\varphi_{q,Q}\rangle;$$
$$G(\Delta E) = \langle\varphi_{q,Q}|\hat{K}(q,Q) + \hat{G}(q,Q;\Delta E)|\varphi_{q,Q}\rangle \qquad (3.1)$$

where it is understood that $G(\Delta E)$ is the system free energy, as a function of the solvent coordinate, for the quantized proton and H-bond vibrations in their ground vibrational states. Here $\hat{K}(q,Q)$ is the full quantum kinetic energy operator which includes $q-Q$ coupling.[28]

The points calculated via eq 3.1 reproduce those already displayed in Figure 5 for the ground state. Further, the line through those points is just the FER eq 1.3, calculated as indicated in the Figure 5 caption. The validity of eq 1.3 having been established, the remaining task is to analyze and provide analytical expressions for its ingredients $\Delta G^{\ddagger}_{o}$, α_o, and α'_o, taken up in the next subsections.

3a. Analysis of $\Delta G^{\ddagger}$ Components. The ground-state free energy resulting from eq 3.1 can be decomposed in a fashion similiar to that described in I for the fixed Q case (section 5 of I)

$$G(\Delta E) = G_{min}(\Delta E) + ZPE(\Delta E) \qquad (3.2)$$

Here, $G_{min}(\Delta E)$ is the full system free energy $G_q(q,Q;\Delta E)$ evaluated at the proton q_{min} and H-bond coordinate Q_{min} values that simultaneously minimize G_q at a given ΔE value

$$\frac{\partial G_q(q,Q;\Delta E)}{\partial q} = 0; \frac{\partial G_q(q,Q;\Delta E)}{\partial Q} = 0 \qquad (3.3)$$

The ZPE is that of the proton *plus* that of the H-bond vibration, i.e., the quantized ground-state vibrational energy in both coordinates with respect to the minimum, at q_{min} and Q_{min}, at any given ΔE.

Figure 8 shows the ground-state free energy curve for the symmetric (a) and an exothermic reaction (b); an endothermic reaction is obviously described by the reverse of Figure 8b. As per eq 3.3, the free energy is decomposed into G_{min} (lower curves in Figure 8a and 8b) and ZPE (Figure 8c). As in the fixed Q case, G_{min} varies with the reaction asymmetry, i.e., finite ΔG_{RXN}, whereas ZPE remains independent of asymmetry. The positions of the critical points in Figure 8 are again described by eq 2.1, except that $\langle c_I^2\rangle$ is now to be interpreted as quantum-averaged over the ground-state wave function describing both the H-bond and proton zero-point vibrations (cf. Figure 3b (solid line)).

From this point forward, the analytic analysis of $G(\Delta E)$ including the quantized H-bond vibrational motion parallels *precisely* that given in section 5 of I for the fixed Q case, and thus, the results are exactly those recounted in the Introduction of the present paper (eqs 1.3−1.5). Accordingly, we limit our discussion to the altered meaning of the quantities appearing in those equations, and in particular to how the properties of G_{min} and ZPE and ultimately G are affected by the H-bond vibration's inclusion.

3b. Brønsted Coefficient and its Derivative. As in I, the expression for the Bronsted coefficient α ultimately derives from the change of the quantum-averaged ionic character $\langle c_I^2\rangle$ between the TS and R compared to the full change between P and R (cf. eq 4.4. of I)

$$\alpha = \partial\Delta G^{\ddagger}/\partial\Delta G_{RXN} = \frac{\langle c_I^2\rangle^{\ddagger} - \langle c_I^2\rangle^{R}}{\langle c_I^2\rangle^{P} - \langle c_I^2\rangle^{R}} \qquad (3.4)$$

Here, the quantum average is taken over the ground vibrational state q, Q wave function. The validity of eq 3.4 is shown in Figure 9, where the line is the numerical derivative of the FER for the ground H-bond vibrational state in Figure 5, and the points are eq 3.4 evaluated for the ground H-bond state of the systems used in Figure 5. This validity reemphasizes the physical correlation made in I that α is related to the similarity in electronic structure between R and TS. As in I, the quantum-averaged electronic structure for the TS of a symmetric reaction is halfway between R and P, $\alpha_o = 0.5$, and α increases starting with $\alpha < 0.5$ for exothermic reactions going toward endothermic

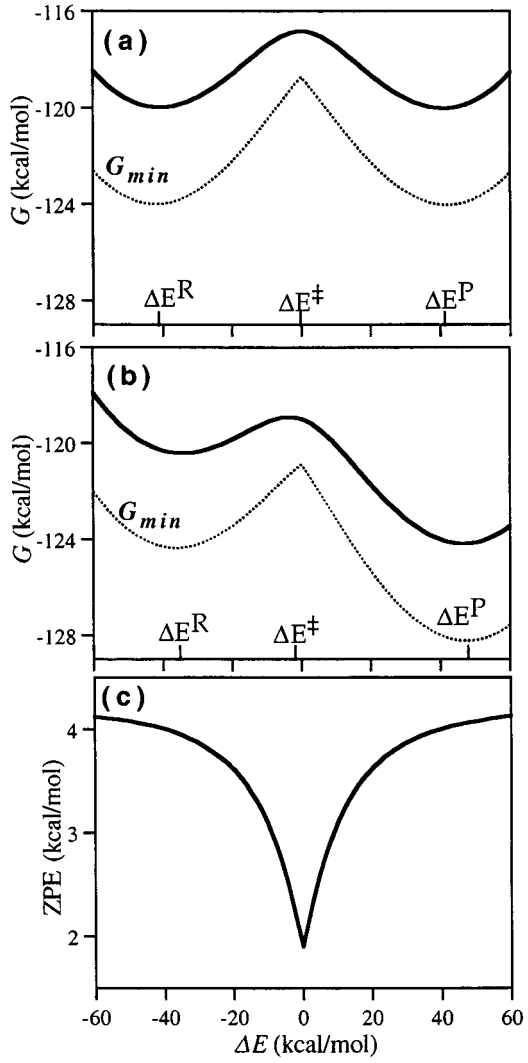

Figure 8. Ground-state free energy curves (solid lines) with both the proton and H-bond vibrations quantized: (a) symmetric reaction and (b) exothermic reaction. Dashed lines show the free energy curves G_{min} excluding the zero point energy (ZPE). (c) ZPE for the proton plus H-bond vibration vs ΔE. The dashed curves in (a) and (b) plus the ZPE in (c) give the full free energy G, solid curves in (a) and (b). ΔE^R, ΔE^P, and $\Delta E^‡$ denote the reactant, product, and transition state solvent configurations, respectively.

reactions where $\alpha > 0.5$. In particular, the structure of eq 3.4 is consistent with the Hammond postulate[29] applied to the electronic structure, indicating that the TS electronic structure becomes more similar to that in the reactant (product) state as the reaction becomes more exothermic (endothermic).

The derivative of the Brønsted coefficient for the symmetric reaction α'_o in eq 1.5, repeated here for convenience

$$\alpha'_o = \left(\frac{1}{k^‡} + \frac{1}{k_R}\right)\frac{1}{(\Delta E^P - \Delta E^R)^2} \tag{3.5}$$

is determined by several ingredients. The first is the sum of the inverses of $k^‡$, the magnitude of the force constant of G at the TS $\Delta E^‡$, and k^R, the force constant for G in the stable reactant well ΔE^R. The remaining factor in α'_o is the inverse square of $\Delta\Delta E = \Delta E^P - \Delta E^R$, the distance in the solvent coordinate between the product and reactant minima in G. From Figure 9, $\alpha'_o = 0.03$ mol/kcal, which is one-half of the value with the H-bond mode fixed ($\alpha'_o = 0.06$ mol/kcal). This reduction is

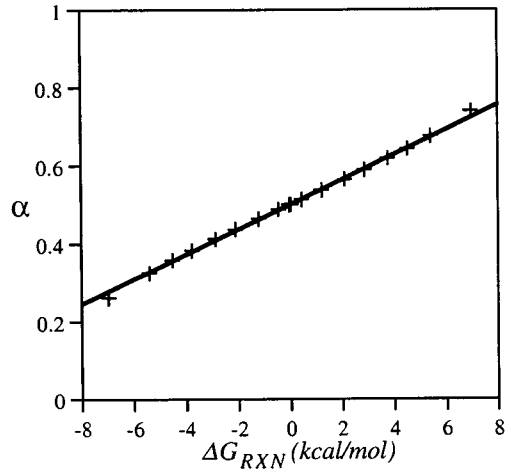

Figure 9. Brønsted coefficient α versus reaction asymmetry. Displayed are the numerical interpolation from the H-bond ground vibrational state FER in Figure 5 (line) and the calculated analytical expression eq 3.4 (+).

predominantly due to the larger solvent rearrangement distance ($\Delta E^P - \Delta E^R$) involved when the H-bond vibration is included, as discussed in section 2a.

3c. Intrinsic Barrier $\Delta G^‡_o$. The two ingredients of the intrinsic barrier eq 1.4, repeated here for convenience

$$\Delta G^‡_o = \Delta G^‡_{m,o} + Z^‡_o - Z_o{}^R \tag{3.6}$$

are a ZPE change and a contribution $\Delta G^‡_{m,o}$ arising from G_{min}, which are now discussed in turn.

3c.1. ZPE Contribution. The ZPE contribution to the intrinsic free energy barrier $\Delta G^‡_o$ is the difference in ZPE between the TS and R: $\Delta ZPE = Z^‡ - Z^R$. Its numerical impact of ΔZPE on $\Delta G^‡_o$ is quite significant: $\Delta G^‡_o = 3.16$ kcal/mol $= \Delta G^‡_{m,o} + \Delta ZPE = 5.26$ kcal/mol-2.1 kcal/mol. This reduction arising from the overall decrease of the total ZPE (proton plus H-bond coordinate) on going from R to TS is mitigated by the feature that the H-bond frequency is higher —approximately double— at the TS than for R, as discussed in section 2b, with a positive H-bond contribution to $\Delta ZPE \approx 0.4$ kcal/mol.

It is perhaps a bit surprising that the numerical value of ΔZPE with both q and Q quantized (−2.1 kcal/mol) hardly differs from that (−2.0 kcal/mol) calculated in I, where only the proton motion is quantized. This results from a near compensation of the H-bond's effect discussed above, involving a higher ZPE for Q in the TS compared to R, with a certain increase of the ZPE in R. The latter arises from the feature that in the present case, the R H-bond coordinate is $Q \approx 2.7$ Å, compared to the fixed $Q = 2.55$ Å value in I. At the larger Q value, the R region is characterized by less ionic character (cf. Figure 3b), with a smaller red shift of the AH proton vibrational frequency, and thus, there is a larger proton ZPE contribution compared to the $Q = 2.55$ Å situation.

3c.2. $\Delta G^‡_{m,o}$. It remains to describe $\Delta G^‡_{m,o}$, the barrier height of G_{min} for the symmetric reaction (Figure 8a, dotted line) (recall that G_{min} is $G(q_{min},Q_{min},\Delta E)$). We first deal with its magnitude, and then pass to an analytic description. The numerical value is $\Delta G^‡_{m,o} = 5.26$ kcal/mol, compared to the corresponding result 3.76 kcal/mol for fixed $Q = 2.55$ Å. As will be seen in more detail below, the larger value when the H-bond vibration is included has its ultimate source in the fact that the distance in the solvent coordinate from the reactant minimum to the TS

$\Delta E = 0$, is larger $0 - (-42$ kcal/mol$) = 42$ kcal/mol compared with $0 - (-35$ kcal/mol$) = 35$ kcal/mol for fixed $Q = 2.55$ Å, and thus more solvent reorganization is required. This larger distance arises from the fact that for the reactant Q value here, $Q = 2.7$ Å (at $\Delta E = -42$ kcal/mol) the ionic character is smaller $c_I^2 = 0.07$ (Figure 3b) than in the fixed $Q = 2.55$ Å case, where the corresponding value (at $\Delta E = -35$kcal/mol) is 0.15 (cf. Figure 5b of I). At the larger Q value, the resonance coupling mixing the two VB states is smaller and less ionic character is produced. (As will be seen, the above discussion must be qualified by a consideration of the ionic character at $\Delta E = 0$, but nonetheless it contains the key points.)

Just as was the case in I, $\Delta G^{\ddagger}_{m,o}$ is the most difficult ingredient to characterize accurately in an analytical fashion. By following exactly the analogous procedures in section 5a.3 of I, it can be analytically approximated by

$$\Delta G^{\ddagger}_{m,o} = \frac{\lambda_m}{4} - \frac{1}{6}\frac{(\Delta E^P_m - \Delta E^R_m)^3}{8}\frac{\partial^2 c_I^2}{\partial \Delta E^2}\bigg|_{\Delta E_m{}^R} \qquad (3.7)$$

in which the first contribution involves the reorganization energy

$$\lambda_m = \frac{1}{2}k_m(\Delta E^P_m - \Delta E_m{}^R)^2 \qquad (3.8)$$

where k_m is the force constant in the reactant G_{min} well (eq 5.8 of I). The second, anharmonic correction in eq 3.7 will be discussed below.

A key aspect of λ_m, just as was discussed in section 5a.3 of I, is that the solvent reorganization it reflects occurs in the presence of the *fixed* ionic character present at ΔE^R_m. The value of $\lambda_m/4$ is 6.98 kcal/mol, which is noticeably larger than the fixed $Q = 2.55$ Å value in I, 4.4 kcal/mol. This increase is completely dominated by the differing distances $\Delta E(=0) - \Delta E^R_m = (\Delta E^P_m - \Delta E^R_m)/2$, completely consistent with our discussion above. But $\lambda_m/4 = 6.98$ kcal/mol is significantly higher ($\sim$33%) than the numerical value $\Delta G^{\ddagger}_{m,o} = 5.26$ kcal/mol, and this difference reflects important anharmonic corrections, evident in Figure 8a, where the double parabolic character of G_{min} is seen to be approximate. This anharmonicity arises, as in I, from the feature that in the presence of strong electronic coupling, the ionic character increases from that at the reactant value at ΔE^R_m to a higher value at $\Delta E = 0$; Figure 3b shows this is a substantial increase (dotted line). Because at $\Delta E = 0$, c_I^2 has increased, *less* solvent reorganization is involved, and so $\Delta G^{\ddagger}_{m,o}$ will be less than $\lambda_m/4$. The most important source of this c_I^2 increase is revealed by Figure 10, which compares $c_I^2(q_{min},Q_{min})$ from Figure 3b with c_I^2 holding either q_{min}, Q_{min}, or q_{min} and Q_{min} fixed going from R to TS. In particular, Figure 10 shows that the increasing c_I^2 is mainly associated with the H-bond coordinate, rather than with the proton coordinate, a behavior consistent with the electronic coupling's exponential increase as (here) Q_{min} decreases from $Q_{min} = 2.7$ Å to $Q_{min} = 2.5$ Å.

The derivation of the analytic anharmonic correction given in eq 3.7, which is only the leading order correction, is detailed in Appendix A. Its value, $= -1.12$ kcal/mol, reduces $\Delta G^{\ddagger}_{m,o}$ to a predicted 5.86 kcal/mol, which is an overestimate of only $\sim$11%, rather than the 33% overestimate provided solely by $\lambda_m/4$.

In summary, eq 3.7 provides a reasonably accurate expression for the intrinsic barrier component $\Delta G^{\ddagger}_{m,o}$ in eq 3.6 for $\Delta G^{\ddagger}_o$, which incorporates a variety of effects described above related to the strong electronic coupling in the system and the H-bond

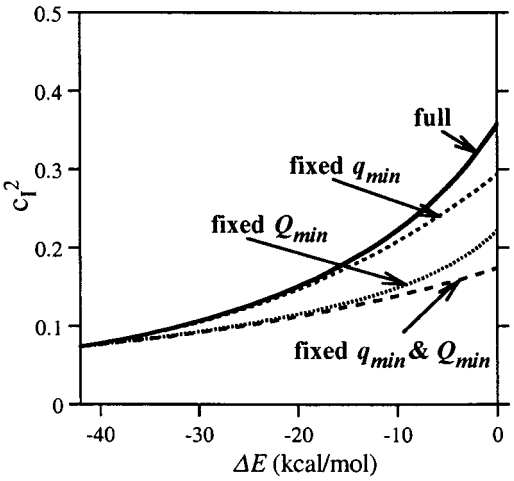

Figure 10. $c_I^2(q_{min},Q_{min};\Delta E)$ versus solvent coordinate going from $\Delta E = -\Delta E_o = -42$ kcal/mol to $\Delta E = 0$ (solid line). For comparison, c_I^2 is plotted for q_{min}, fixed (small dash), Q_{min} fixed (dotted line), and both Q_{min} and q_{min}, fixed (large dash). See text for discussion.

-solvent coupling. It is worth stressing that the H-bond coordinate's influence described above is quite different from what could be termed an H-bond reorganization energy, analogous to outer sphere vibrational coordinate contributions in electron transfer theory;[30] in the model system treated, the equilibrium separations and frequencies of the H-bond in the reactant and product are taken to be the same, and no such contribution can arise.[31]

3d. Free Energy Relationship. We have already seen in Figure 5 that the FER eq 1.3 is an excellent description for the ground H-bond vibrational state PT reaction (which itself accounts for almost all of the free energy behavior). We now examine how the analytic representations discussed in sections 3b and 3c for the intrinsic barrier $\Delta G^{\ddagger}_o$, eq 1.4, and the Bronsted coefficient derivative α'_o, eq 1.5, fare numerically in describing the FER, always within the context of eq 1.3.[32] (The symmetric reaction Bronsted coefficient value is always $\alpha_o = 0.5$ for the systems considered here).

We examine this in two steps in Figure 11a in comparing with eq 1.3, repeated here

$$\Delta G^{\ddagger} = \Delta G^{\ddagger}_o + \alpha_o \Delta G_{RXN} + \alpha'_o \frac{(\Delta G_{RXN})^2}{2} \qquad (3.9)$$

whose numerical ingredients were already determined in Figure 5 via a fit; $\Delta G^{\ddagger}_o = 3.16$ kcal/mol, and $\alpha'_o = 0.032$ mol/kcal. First (solid line), we employ the analytical results eqs 3.6 and 3.7, and eq 3.5 for both $\Delta G^{\ddagger}_o$ and α'_o, respectively: $\Delta G^{\ddagger}_o = 3.76$ kcal/mol and $\alpha'_o = 0.03$ mol/kcal. Second (dotted line), we instead use the numerical fit value for $\Delta G^{\ddagger}_o$ and the analytical value for α'_o, namely $\Delta G^{\ddagger}_o = 3.16$ kcal/mol and $\alpha'_o = 0.03$ mol/kcal. In the first case, the completely analytic treatment correctly gives the shape of the FER curve, but is uniformly high, an error due almost exclusively to the analytical overestimate of the intrinsic barrier by about 20%. As discussed in section 3c, this is due to the error in the analytic approximation eq 3.7 for the intrinsic barrier component $\Delta G^{\ddagger}_{m,o}$, which could be reduced as the expense of much more complex calculations. In the second case, this shortcoming is repaired by simply using the numerical fit value for $\Delta G^{\ddagger}_o$, and it is seen that the agreement with the full FER curve is excellent.

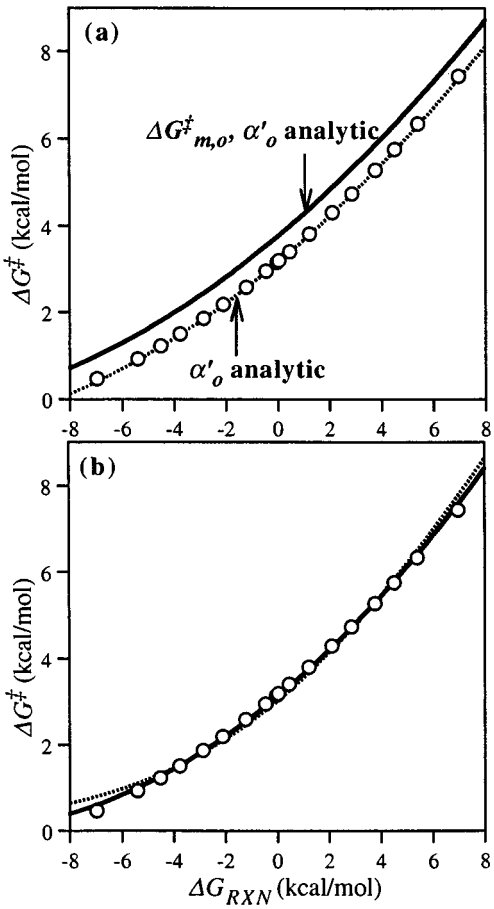

Figure 11. (a) Points are the free energy behavior for the ground H-bond vibrational state taken from Figure 5. Solid line is eq 3.9 with $\Delta G^{\ddagger}_o = 3.76$ kcal/mol, $\alpha_o = 0.5$, and $\alpha'_o = 0.03$ mol/kcal. Dotted line is eq 3.9 with $\Delta G^{\ddagger}_o = 3.16$ kcal/mol, $\alpha_o = 0.5$, and $\alpha'_o = 0.03$ mol/kcal. (b) Same points as in (a), and the solid line is the fit to the Marcus FER (eq 3.10, $\Delta G^{\ddagger}_o = 3.12$ kcal/mol), whereas dotted line is the fit to the BEBO FER (eq 3.11, $\Delta G^{\ddagger}_o = 3.02$ kcal/mol).

A similar excellent agreement with the full FER is shown in Figure 11b (solid line) for the empirical Marcus FER[2]

$$\Delta G^{\ddagger} = \Delta G^{\ddagger}_o + \frac{\Delta G_{RXN}}{2} + \frac{(\Delta G_{RXN})^2}{16\Delta G^{\ddagger}_o} \qquad (3.10)$$

which involves a numerical fit for $\Delta G^{\ddagger}_o$ (= 3.12 kcal/mol) in this equation. Within the context of a quadratic FER, this success occurs for precisely the same reasons discussed at length in section 5d of I. In particular, $\Delta G^{\ddagger}_o$ is numerically fit to give the correct symmetric reaction barrier, the Brønsted coefficient is 0.5 for the symmetric reaction, and the influence of the FER curvature determined by α'_o, eq 3.5, is not pronounced in the present systems, so that the relation $\alpha'_o = 1/8\Delta G^{\ddagger}_o$ enforced by the Marcus relation is a good enough numerical estimate when compared to the numerically fit value $\alpha'_o = 0.8/8\Delta G^{\ddagger}_o$ for the full FER. We remind the reader that, as described in appendix B of I, α'_o can be empirically represented by the numerical relation $\alpha'_o = f/8\Delta G^{\ddagger}_o$, where f is a numerical factor, though there is *no* fundamental relation connecting α'_o and $\Delta G^{\ddagger}_o$.

To reinforce the main point concerning the insensitivity to the FER curvature, we briefly discuss another FER which also has $\Delta G^{\ddagger}_o$ as its only parameter

$$\Delta G^{\ddagger} = \Delta G_{RXN} - \Delta G^{\ddagger}_o \ln(n^{\ddagger})/\ln(2) \qquad (3.11)$$

which was derived for gas-phase PT from the BEBO perspective by Marcus[2] and further analyzed by Agmon and Levine,[33] and recently employed for excited-state PT in solution.[5] Here $n^{\ddagger}$ is the bond order at the TS

$$n^{\ddagger} = 1/[1 + \exp(-\Delta G_{RXN} \ln 2/\Delta G^{\ddagger}_o)] \qquad (3.12)$$

Figure 11b shows that the numerical fit (dotted line, with $\Delta G^{\ddagger}_o = 3.02$ kcal/mol) of eq 3.11 is in quite good agreement with the full FER. The numerical agreement is not as good as with the Marcus eq 3.10 because eq 3.11 contains a more sensitive second order dependence $\alpha'_o = 2 \ln 2/8\Delta G^{\ddagger}_o) = 1.4/(8\Delta G^{\ddagger}_o)$ compared to $\alpha'_o = 1/(8\Delta G^{\ddagger}_o)$ in eq 3.10. However, both are comparable with the empirical value $\alpha'_o = 0.8/(8\Delta G^{\ddagger}_o)$ numerically found from the full FER. Despite the numerical overestimation (20% by the Marcus FER and 75% by the BEBO FER), and the quite differential conceptual basis of α'_o in these descriptions compared to our eq 3.5, both FERs present reasonable fits because the curvature of the full FER is not pronounced, only becoming visible for the extreme values of reaction asymmetry. It is however worth stressing in this connection that, in contrast to the present development, the underlying contributions to the intrinsic barrier are not given in either the Marcus or the Agmon−Levine BEBO relations.

An experimental distinction between eq 3.10 and eq 1.3 would obviously be desirable. On the basis of the discussion above, this distinction would depend strongly on the accuracy of the curvature in FER plots, and unfortunately not enough data of sufficient precision currently exists. This possible distinction will be discussed further in future work[34] in connection with kinetic isotope effect behavior versus reaction asymmetry for PT reactions.

3e. Other PT Free Energy Relationships. There are several other FERs in the literature as applied to PT: the first[4,7,19] is based on an underlying electronically diabatic perspective, whereas the second[13,18,20] is expressed in a proton diabatic description. We now discuss these in turn.

As discussed in the Introduction of I, the Marcus relation eq 3.10 originally arose in connection with weak electronic coupling electron transfer (ET) reactions,[30] and in that context, the intrinsic reaction barrier $\Delta G^{\ddagger}_o$ is given by 1/4 of a reorganization energy, based on an underlying electronically *diabatic* picture. This reorganization energy is defined[30] by the free energy difference associated with a Franck−Condon excitation from the equilibrium reactant position for the reactant electronic diabatic state to the product electronic diabatic state, followed by the relaxation, in a solvent coordinate along the product diabatic curve, to the equilibrium product position.

The modified FER appropriate for the electronically adiabatic ET limit—and still framed in terms of a reorganization energy rather than an intrinsic reaction barrier—has been developed,[4,19,35] and has been used to describe the free energy behavior not only for ET, but also for a variety of charge-transfer reactions in a polar environment involving bond-making and -breaking, including PT[4,7,19]

$$\Delta G^{\ddagger} \approx \frac{(\lambda + \Delta G_{RXN})^2}{4\lambda} - \beta^{\ddagger} + \frac{(\beta^R)^2}{(\lambda + \Delta G_{RXN})} \qquad (3.13)$$

Here, λ is an electronically diabatic reorganization energy, now including both solvent and nuclear rearrangement contributions, whereas β^R and $\beta^{\ddagger}$ are the electronic resonance coupling values

evaluated at the reactant and transition state, respectively. The last two terms in eq 3.13 are the leading order corrections to the barrier height due to a finite electronic coupling at TS and R.[4,19,35] In the PT context, eq 3.13 has been employed under conditions where λ far exceeds both ΔG_{RXN} and any relevant electronic coupling, such that only linear $\Delta G^{\ddagger} - \Delta G_{RXN}$ behavior is found.[4,7,19] In this regime, the issue of the Brønsted coefficient variation with reaction asymmetry and the associated Hammond postulate behavior which it quantifies does not arise. More generally, however, eq 3.13 has not been tested to our knowledge and involves some difficulties and complexities. For example, eq 3.13 does not predict a Brønsted coefficient equal to 0.5 for a symmetric reaction.[36] Further, the simple subtraction of the TS value of the coupling to account for resonance lowering of the TS barrier top applies only for a symmetric reaction. In addition, there are hidden dependencies on ΔG_{RXN} in eq 3.13: as ΔG_{RXN} changes, the location of the nuclear coordinates, including the H-bond coordinate Q, for R and TS will shift, and because the electronic coupling is exponentially sensitive to Q variations, there is a strong implicit ΔG_{RXN} dependence in the electronic coupling terms in eq 3.13. All these issues deserve exploration.

A final point regarding eq 3.13 as applied to PT is that the proton is not quantized, i.e., it enters as a classical coordinate, and in that sense corresponds more to the "standard" picture of PT described in I. Although a quantum correction to eq 3.13 exists,[37] the underlying adherence to a "standard" picture formulates all quantum corrections based on a reference classical path,[38] and in such a description, the transition state of a symmetric PT reaction contains no proton quantum correction;[37a] there is no involvement of any proton motion in the ZPE at the transition state,; this strongly contrasts with the present description, where the proton motion is orthogonal to the reaction coordinate, a key difference between the present perspective and the "standard" picture.[39]

Equation 3.13 was derived[4,19,35] via a curve-crossing approach defined by two electronic VB states and their resonance coupling. One can take an alternate curve-crossing approach to proton transfer.[13,18,20] In this approach, the diabatic states in the Hamiltonian are instead *proton* diabatic states, defined as proton eigenstates localized near the donor or acceptor nuclei, and the electronic resonance coupling is replaced by the proton coupling, which is defined as half of the difference in energy between the proton ground and first excited vibrational states at the TS for the symmetric reaction. A reorganization energy is then defined via proton diabatic states on the ground electronically adiabatic surface. The free energy relationship for the curve-crossing picture in the adiabatic PT limit has been described,[13,18,40] and the corrections due to the shift in the position of both the reactant and transition state (necessary for $\Delta G_{RXN} \neq 0$) are explicitly taken into account.[18a,41] In the curve crossing model, however, the ZPE contributions to the free energy surface vital to understanding adiabatic PT are only implicitly present, and their influence is not at all clearly revealed, in contrast to the description here and in I.

4. Concluding Remarks

Here, we have extended the analysis of the previous paper (I) to analyze the nonlinear FER for proton transfer reactions in solution in the quantum proton adiabatic regime to include the important influence of the H-bond coordinate gauging the separation of the proton-donor and -acceptor species. In addition to the proton, the H-bond vibration was quantized in the treatment. In this proton adiabatic regime, the quantum proton vibration adiabatically follows the slower coordinates, including that of the solvent, the latter essentially determining the reaction path and making a significant contribution to the activation free energy. Despite the quite different conceptual basis of the treatment compared to more traditional approaches, we showed that the "path" for the reaction characterized by the values of the quantum-averaged proton and hydrogen bond coordinates—at each value of the solvent coordinate—is very similar to that resulting from a Bond Energy-Bond Order pathway, related to a mode of analysis currently in use for examining the characteristics of the state of hydrogen bonds within potential proton-transfer complexes.

As in I, we could find a quadratic FER (eq 3.9) of the general form often applied in characterizing experimental connections between reaction rates and reaction thermodynamics of proton transfers in polar environments. We have derived approximate analytic expressions for the ingredients of this FER, including the intrinsic reaction barrier (eq 3.6)—the activation free energy for the thermodynamically symmetric reaction, and the quadratic coefficient, related to the variation of the Bronsted coefficient with respect to the thermodynamic reaction asymmetry (eq 3.5). For example, the former is governed by the solvent reorganization, modulated by certain electronic structure changes, and the change in the combined ZPE of the proton and the hydrogen bond vibrations to reach the transition state in the solvent coordinate. The involvement of the proton ZPE in the intrinsic barrier is just one reflection of the strong difference of the present view and the more traditional microscopic conceptions of PT.[1,2,9] In the latter, no such contribution will enter because the proton coordinate is the reaction coordinate, whereas in the present approach, it is instead transverse to the reaction coordinate.

We compared and contrasted our FER with assorted other relations in the literature, and pointed out the limitations of some of the latter. In connection with the most widely applied FER among these—the empirical Marcus equation, we showed that, due to the typically limited accessible range of thermodynamic reaction asymmetries, the numerical differences between our FER and the latter are not pronounced (for the latter, the intrinsic barrier is regarded simply as a parameter to be fit), largely due to the modest numerical impact of the identity of the quadratic coefficient, whose expressions differ fundamentally in the two descriptions. In view of this, the most important result of the present work—beyond the FER itself—is probably the explicit analytic expression for the intrinsic barrier in terms of its microscopic ingredients (cf. eqs 3.6 and 3.7).

There are several restrictions for our treatment within, even within the proton adiabatic regime. One is that we have not included what we have termed "intrinsic asymmetry", which would include for example the feature that even for a thermodynamically symmetric reaction, the H-bond length and frequency may differ for the reactant and the product. This type of restriction will be removed in future work, but our preliminary results indicate that although the analysis is more complicated, the essential character of the results remains unaltered, although new details will appear—such as a hydrogen bond reorganization energy component for the intrinsic barrier. A second restriction is that the underlying electronic structure variations associated with the PT should be approximately describable in terms of two dominant valence bond structures. This kind of description is unlikely to apply for certain proton transfers, notably for those involving carbon acids,[42] whose analysis is reserved for the future. In addition, we have considered only fairly low proton barrier reactions, consistent with relatively fast PT reactions.[1c,5,12,13]

This is an essential requirement for the proton adiabatic regime considered herein, where the ZPE of the proton lies above the proton barrier when the transition state in the solvent coordinate is reached. For reactions where this proton barrier is sufficiently high that this is no longer the case, then nonadiabatic PT, i.e., tunneling (cf. refs 15, 18, and 20), obviously must be included. In one extreme, such as a large proton barrier arising from large hydrogen bond coordinate values (cf. Figure 2 of I), the reaction can be completely tunneling. But more generally, reaction via nonadiabatic PT pathways will be in competition with proton adiabatic pathways, now involving excited proton vibrational levels (as opposed to being in competition with classical, "over the barrier" proton motion; See ref 19 of I). This general situation is the subject of current research.

Finally, we emphasize that we have been able to show that a FER of the type often found to well describe experimental proton transfer reactions follows from a proton adiabatic picture which differs quite fundamentally from the traditional view[1,2,9] of proton-transfer reactions. In a subsequent paper,[34] we will show that the kinetic isotope effect behavior predicted by the proton adiabatic picture is just the behavior often experimentally observed and thought to unequivocally support the traditional picture.

5. Acknowledgments

This work was supported in part by NSF Grants CHE-9700419 and CHE-0108314. PK acknowledges the support of an NIH Postdoctoral Fellowship.

Appendix A: Intrinsic Reaction Barrier for G_{min}

Because the derivation of eq 3.7 for $\Delta G^{\ddagger}_{m,o}$ closely parallels that in appendix A in I, we only highlight the important results. The intrinsic barrier for G_{min} can be written as (eq A.2 in I)

$$G^{\ddagger}_{m,o} = \frac{k_m}{2}\Delta E_o{}^2 - \int_{-\Delta E_o}^{0} d\Delta E' \int_{-\Delta E_o}^{\Delta E'} d\Delta E''\left(\frac{\partial c_I^2(\Delta E'')}{\partial \Delta E''} - \frac{\partial c_I^2(\Delta E'')}{\partial \Delta E''}\Big|_{-\Delta E_o}\right) \quad (A.1)$$

where $\Delta E_o = -\Delta E^R_m$ and $2\Delta E_o = \Delta E^P_m - \Delta E^R_m$ for the symmetric reaction. Here, we have employed a shorthand notation for $c_I^2(q_{min},Q_{min},\Delta E)$, bearing in mind that both Q_{min}, and q_{min} depend on ΔE. Using an expansion of c_I^2 about the minimum of R, eq A.1 can be rewritten as

$$\Delta G^{\ddagger}_{m,o} = \frac{k_m}{2}\Delta E_o^2 - \frac{C}{6}\Delta E_o{}^3 \quad (A.2)$$

where C is the second derivative evaluated at the minimum

$$C = \partial^2 c_I^2(\Delta E)/\partial \Delta E^2|_{-\Delta E_o} \quad (A.3)$$

and k_m depends on the first derivative of c_I^2 and the electronically diabatic force constant k_d (cf. eq 5.8 of I)

$$k_m = k_d - \frac{\partial c_I^2}{\partial \Delta E}|_{\Delta E_m{}^R} \quad (A.4)$$

The first derivative of c_I^2 is

$$\frac{\partial c_I^2}{\partial \Delta E} = \frac{2c_I^3\, c_N^3}{\beta}\left[1 + \frac{\partial \Delta U}{\partial \Delta E} - \frac{(c_I^2 - c_N^2)}{c_I c_N}\frac{2\beta}{\partial \Delta E}\right] \quad (A.5)$$

which includes variation in the electronic coupling due to the Q_{min} change with ΔE. The derivatives with respect to ΔE can be written in terms of forces due to nuclear gradients multiplied by the nuclear coordinate variation with respect to ΔE

$$\frac{\partial \Delta U}{\partial \Delta E} = \frac{\partial V_N}{\partial \Delta E} - \frac{\partial V_I}{\partial \Delta E} = \frac{\partial V_N}{\partial q}\frac{\partial q_{min}}{\partial \Delta E} - \frac{\partial V_I}{\partial \tilde{q}}\frac{\partial \tilde{q}_{min}}{\partial \Delta E}$$

$$= -F_{N,q}\frac{\partial q_{min}}{\partial \Delta E} + F_{I,\tilde{q}}\frac{\partial \tilde{q}_{min}}{\partial \Delta E} \quad (A.6)$$

$$\frac{\partial \beta}{\partial \Delta E} = \frac{\partial \beta}{\partial Q}\frac{\partial Q_{min}}{\partial \Delta E} = -F_{\beta,Q}\frac{\partial Q_{min}}{\partial \Delta E} \quad (A.7)$$

with the notation in eq A.6 for the proton−proton acceptor distance (H···B) $\tilde{q} = Q - q$ ($\tilde{q}_{min} = Q_{min} - q_{min}$). The second derivative of c_I^2 is

$$\frac{\partial^2 c_I^2}{\partial \Delta E^2} = \frac{2c_I^3\, c_N^3}{\beta^2}\left\{\beta\frac{\partial^2 \Delta U}{\partial \Delta E^2} - \beta\frac{(c_I^2 - c_N^2)}{c_I c_N}\frac{\partial^2 \beta}{\partial \Delta E^2} - 3c_I c_N(c_I^2 - c_N^2)\left(1 + \frac{\partial \Delta U}{\partial \Delta E}\right)^2 + 4\frac{\partial \beta}{\partial \Delta E}\left(1 + \frac{\partial \Delta U}{\partial \Delta E}\right)(1 - 6c_I^2\, c_N^2) - \frac{(c_I^2 - c_N^2)}{c_I c_N}\left(\frac{\partial \beta}{\partial \Delta E}\right)^2(1 - 12c_I^2\, c_N^2)\right\} \quad (A.8)$$

There are two types of contribution to the derivatives of c_I^2: mixing of electronic diabatic states and nuclear coordinate shifts. Neglecting nuclear gradient terms, eqs. A.5 and A.8 become

$$\frac{\partial c_I^2}{\partial \Delta E} = \frac{2c_I^3\, c_N^3}{\beta};\ \frac{\partial^2 c_I^2}{\partial \Delta E^2} = \frac{6c_I^4\, c_{N4}}{\beta^2}(c_N{}^2 - c_I^2) \quad (A.9)$$

The harmonic term in eq A.2, with eqs. A.4 and A.5, is 6.98 kcal/mol, and the anharmonic term in A.2, using eqs. A.3 and A.8, is-1.12 kcal/mol, resulting in $\Delta G^{\ddagger}_{m,o} = 5.86$ kcal/mol. For comparison, use of the approximations for the ionic character derivatives eq. A.9, the harmonic term is 7.76 kcal/mol, and the anharmonic term is −0.4 kcal/mol, giving $\Delta G^{\ddagger}_{m,o} = 7.76 - 0.4 = 7.36$ kcal/mol. This indicates that the nuclear shifts reduce $\Delta G^{\ddagger}_{m,o}$ by ∼25%.

References and Notes

(1) (a) Bell, R. P. *The Proton in Chemistry*, 2nd ed.; Cornell University Press: Ithaca, NY, 1973. (b) Caldin, E.; Gold, V. *Proton-Transfer Reactions*; Chapman and Hall: London, 1975. (c) Kresge, A. J. *Acc. Chem. Res.* **1975**, *8*, 354. (d) Kresge, A. J. In *Isotope Effects on Enzyme-Catalyzed Reactions*; Cleland, W. W., O'Leary, M. H., Northrop, D. B., Eds.; University Park Press: Baltimore, MD, 1977; p 37.

(2) (a) Marcus, R. A. *Faraday Symp. Chem. Soc.* **1975**, *10*, 60. (b) Marcus, R. A. *J. Phys. Chem.* **1968**, *72*, 891. (c) Cohen, A. O.; Marcus, R. A. *J. Phys. Chem.* **1968**, *72*, 4249. (d) Marcus, R. A. *J Am. Chem. Soc.* **1969**, *91*, 7224.

(3) (a) Kreevoy, M. M.; Konasewich, D. E. *Adv. Chem. Phys.* **1972**, *21*, 243. (b) Kreevoy, M. M.; Oh, S.-w. *J. Am. Chem. Soc.* **1973**, *95*, 4805.

(4) Warshel, A. *Computer Modeling of Chemical Reactions in Enzymes and Solutions*; John Wiley and Sons: New York, 1991.

(5) Pines, E.; Magnes, B.-Z.; Lang, M. J.; Fleming, G. R. *Chem. Phys. Lett* **1997**, *281*, 413.

(6) **(a)** Kresge, A. J.; Silverman, D. N. *Methods Enzymol.* **1999**, *308*, 276. **(b)** Gerlt, J. A.; Gassman, P. G. *J. Am. Chem. Soc.* **1993**, *115*, 11 552.

(7) (a) Kong, Y. S.; Warshel, A.; *J. Am. Chem. Soc.* **1995**, *117*, 6234. (b) Warshel, A.; Schweins, T.; and Fothergil, M. *J. Am. Chem. Soc.* **1994**, *116*, 8437. (c) Schweins, T.; Warshel, A.; *Biochemistry* **1996**, *35*, 14 232.

(8) Kiefer, P. M.; Hynes, J. T. *J. Phys. Chem. A* **2002**, *106*, 1834.

(9) Melander, L.; Saunders: W. H. *Reaction Rates of Isotopic Molecules*; John Wiley and Sons: New York, 1980.

(10) (a) Mulliken, R. S. *J. Phys. Chem.* **1952**, *56*, 801. (b) Mulliken, R. S.; Person, W. B. *Molecular Complexes*; John Wiley and Sons: New York, 1969. (c) Mulliken, R. S. *J. Chim. Phys.* **1964** , *20*, 20.

(11) Timoneda, J. J.; Hynes, J. T. *J. Phys. Chem.* **1991**, *95*, 10 431.

(12) (b) Ando, K.; Hynes, J. T. *J. Phys. Chem. A* **1999** *103*, 10 398. (b) Ando, K.; Hynes, J. T. *J. Phys. Chem. B* **1997**, *101*, 10 464.

(13) Staib, A.; Borgis, D.; Hynes, J. T. *J. Chem. Phys.* **1995**, *102*, 2487.

(14) The treatment of ref 13 utilizes a curve-crossing formalism, in which the solvent−H-bond coordinate coupling arises from the mixing of the proton nuclear diabatic states, as opposed to the electronic mixing described here and in I. The curve-crossing picture can be recovered from the present picture by extracting the proton coupling from the proton potentials. The link between the two is provided by the fact that the electronic coupling determines the proton potentials which in turn determine the proton coupling.

(15) (a) Basilevsky, M. V.; Soudackov, A.; Vener, M. V. *Chem. Phys.* **1995**, *200*, 87. (b) Basilevsky, M. V.; Vener, M. V.; Davidovich, G. V.; Soudackov, A. *Chem. Phys.* **1996**, *208*, 267. (c) Vener, M. V.; Rostov, I. V.; Soudackov, A.; Basilevsky, M. V.; *Chem. Phys.* **2000**, *254*, 249.

(16) (a) Steinet, T.; Saenger, W. *Acta Crystallog. Sec. B* **1994**, 348. (b) Steinet, T. *J. Chem. Soc., Chem. Commun.* **1995**, 1331.

(17) (a) Smirnov, S. N.; Benedict, H.; Golubev, N. S.; Denisov, G. S.; Kreevoy, M. M.; Schowen, R. L.; Limbach, H.-H. *Can. J. Chem.* **1999**, *77*, 943. (b) Benedict, H.; Limbach, H.-H.; Wehlan, M.; Fehlhammer, W.-P.; Golubev, N. S.; Janoscheck, R. *J. Am. Chem. Soc.* **1998**, *120*, 2939.

(18) (a) Borgis, D.; Hynes, J. T. *J. Phys. Chem.* **1996**, *100*, 1118. (b)-Borgis, D.; Hynes, J. T. *Chem. Phys.* **1993**, *170*, 315. (c) Borgis, D.; Lee, S.; Hynes, J. T. *Chem. Phys. Lett.* **1989**, *162*, 19. (d) Lee, S.; Hynes, J. T. *J. Chim. Phys.* **1996**, *93*, 1783.

(19) (a) Åqvist, J.; Warshel, A. *Chem. Rev.* **1993**, *93*, 2523. (b) Hwang, J.-K.; King, G.; Creighton, S.; Warshel, A. *J. Am. Chem. Soc.* **1988**, *110*, 5297. (c) Warshel, A.; Hwang, J.-K.; *Faraday Discuss.* **1992**, *93*, 225.

(20) (a) Dogonadze, R. R.; Kuznetzov, A. M.; Levich, V. G. *Electrochim. Acta* **1968**, *13*, 1025. (b) German, E. D.; Kuznetzov, A. M.; Dogonadze, R. R. *J. Chem. Soc., Faraday Trans. 2* **1980**, *76*, 1128. (c) Ulstrup, J. *Charge-Transfer Processes in Condensed Media*; Springer: Berlin, 1979. (d) Kuznetzov, A. M. *Charge Transfer in Physics, Chemistry and Biology: Physical Mechanisms of Elementary Processes and an Introduction to the Theory*; Gordon and Breach Pubs.: Amsterdam, 1995. (e) Kuznetzov, A. M. and Ulstrup, J. *Can. J. Chem.* **1999**, *77*, 1085. (f) Sühnel, J.; Gustav, K. *Chem. Phys.* **1984**, *87*, 179.

(21) Pimentel, G. C.; McClellan, A. L. *The Hydrogen Bond*; W. H. Freeman: New York, 1960.

(22) This feature is absent in the model calculations of ref 13, in which the basic model Hamiltonian is not constructed quantum mechanically, and the electronic coupling does not enter explicitly, and thus effects due to its variation are absent.

(23) The higher H-bond frequency potential at $\Delta E = 0$ has been characterized in an alternate, but ultimately equivalent perspective in Staib et al.[13,14]

(24) One could wonder, if the H-bond mode Q of frequency 300−500 cm^{-1} is quantized, whether it is consistent to treat the solvent coordinate as classical, since water and other protic solvents have active librational modes of several hundred cm^{-1}. As discussed in section 2, the question would be most relevant in the key TS region (in section 2, $\omega_Q > 500\ cm^{-1}$). Indeed, one might wish to quantize a portion of these librations in a more sophisticated treatment. However, this would require the introduction of more than one solvent coordinate in the analysis, and it is likely to be only worth doing in connection with a detailed realistic computer simulation.

(25) Pauling, L. *J. Am. Chem. Soc.* **1947**, *69*, 542.

(26) This corner-cutting aspect is similar to that common in various discussions typically focused on gas-phase H atom transfer,[27] where the quantum particle tunnels through the barrier in its coordinate.

(27) (a) Babamov, V. K.; Marcus, R. A. *J. Chem. Phys.* **1981**, *74*, 1790. (b) Hiller, C.; Manz, J.; Miller, W. H.; Römelt, J. *J. Chem. Phys.* **1983**, *74*, 3850. (c) Miller, W. H. *J. Am. Chem. Soc.* **1979**, *101*, 6819. (d) Skodje, R. T.; Truhlar, D. G.; Garrett, B. C. *J. Chem. Phys.* **1982**, *77*, 5955. (e) Marcus, R. A.; Coltrin, M. E. *J. Chem. Phys.* **1977**, *67*, 2609. (f) Garrett, B. C.; Truhlar, D. G. *J. Chem. Phys.* **1983**, *79*, 4931. (g) Kim, Y.; Kreevoy, M. M. *J. Am. Chem. Soc.* **1992**, *114*, 7116.

(28) For a quantitative description, the kinetic coupling between Q and q is an important aspect of heavy-light-heavy systems (see, e.g., eq 8−21 in J. I. Steinfeld; J. S. Francisco; W. L. Hase "Chemical Kinetics and Dynamics", Prentice Hall: New Jersey, 1989.) Even with the $q-Q$ kinetic coupling, the eigenstates are qualitatively similar to and the eigenvalues are numerically close to those obtained with the successive BO result. For the latter, the proton is quantized first, followed by that of the H-bond vibration; $G(\Delta E)$ would be then given by the expectation value $G(\Delta E) = \langle\Phi_o(Q;\Delta E)|\langle\phi_o(q;Q,\Delta E)|\hat{K}_q + \hat{K}_Q + G_q(q,Q;\Delta E)|\phi_o(q;Q,\Delta E)\rangle|\Phi_o(Q;\Delta E)\rangle$, where the ground-state wave functions for Q and q are taken from eq 2.5 and eq 2.13 in I, respectively.

(29) (a) Hammond, G. S. *J. Am. Chem. Soc.* **1955**, *77*, 334. (b) Lowry, T. H.; Richardson, K. S. *Mechanism and Theory in Organic Chemistry*, 3rd ed.; Harper Collins Publishers: New York, 1987.

(30) (a) Marcus, R. A. *J. Chem. Phys.* **1956**, *24*, 979. (b) Marcus, R. A. *J. Chem. Phys.* **1956**, *24*, 966. (c) Marcus, R. A.; Sutin, N. *Biochim. Biophys. Acta* **1985**, *811*, 265. (d) Sutin, N. *Prog. Inorg. Chem.* **1983**, *30*, 441.

(31) The diabatic potential surfaces V_I, V_N, and V_Q used here and in I assume an intrinsic asymmetry, e.g., $V_I(q)=V_N(Q-q)$, the frequencies of the reactant and product diabatic potentials are identical; the equilibrium H-bond separation Q and its frequency are the same in the reactant and product. For real systems, this will obviously not be the case. Nonetheless, preliminary investigations of the FER including intrinsic asymmetry indicate that the FER and its underlying physical interpretation are not significantly altered. In particular, the Brønsted coefficient $\alpha \neq 1/2$ for $\Delta G_{RXN} = 0$ for the intrinsically asymmetric case, but the deviation from 1/2 is small.

(32) A corresponding analysis of the complete thermally activated rate constant could be done with separate but identical decompositions for higher H-bond vibrational states (e.g. $i = 1$), where these relationships would be included with the ground-state case $i = 0$ in eqs 2.7 and 2.8.

(33) (a) Agmon, N.; Levine, R. D. *Chem. Phys. Lett.* **1977**, *52*, 197. (b) Agmon, N.; Levine, R. D. *J. Chem. Phys.* **1979**, *71*, 3034. (c) Agmon, N.; Levine, R. D. *Israel J. Chem.* **1980**, *19*, 330.

(34) Kiefer, P. M.; Hynes, J. T., in preparation.

(35) Sutin, N. *Prog. Inorg. Chem.* **1983**, 30, 441.

(36) Of course, for real systems which are not exchange reactions (e.g., AH···A ⇒ A···HA), α is not expected to be exactly 1/2.[31] However, eq 3.13 does not preclude exchange reactions and hence does not predict a proper Brønsted coefficient.

(37) (a) Hwang, J.-K.; Warshel, A. *J. Phys. Chem.* **1993**, *97*, 10 053. (b) Hwang, J.-K.; Chu, Z. T.; Yadav, A.; Warshel, A. *J. Phys. Chem.* **1991**, *95*, 8445. (c) Hwang, J.-K.; Warshel, A. *J. Am. Chem. Soc.* **1996**, *118*, 11 745.

(38) In addition, variation of quantum corrections along a reaction path will also shift the R, P, and TS locations. As discussed in detail in I, the ZPE variation along the reaction coordinate significantly affects how these locations vary versus reaction asymmetry and consequently impact the resulting FER. Simple addition of ZPE differences to a classically derived FER[37] will thus only be correct for a symmetric reaction.

(39) This aspect will be further discussed in connection with kinetic isotope effects in a future article.[34]

(40) The FER using a curve-crossing picture for nonadiabatic PT tunneling limit was also considered.[18,20]

(41) In contrast to eq 3.13, the analysis in ref 18a gives a proper Bronsted coefficient for a symmetric reaction case, although the analysis is restricted to large solvent reorganization energy.

(42) (a) Agmon, N. *J. Am. Chem. Soc.* **1980**, *102*, 2164. (b) Marcus, R. A. *J. Am. Chem. Soc.* **1969**, *91*, 7224. (c) Bernasconi, C. F. *J. Am. Chem. Soc.* **1997**, *119*, 4008. (d) Bernasconi, C. F. *Acc. Chem. Res.* **1987**, *20*, 301. (e) Bordwell, F. G.; Boyle, W. J., Jr. *J. Am. Chem. Soc.* **1974**, *94*, 3907. (f) Pross, A. *Adv. Phys. Org. Chem.* **1985**, *21*, 99. (g) Pross, A.; Shaik, S. *J. Am. Chem. Soc.* **1982**, *104*, 1129. (h) Baksic, D.; Bertran, J.; Lluch, J. M.; Hynes, J. T. *J. Phys. Chem. A* **1998**, *102*, 3977.